KSTLE International Journal, Vol. 2, No. 1, June 2001, pp. 46-54

A Study on the Air-Lubricated Herringbone Groove Journal Bearing by Finite Element Method

Shin-Wook Park and Yoon-Chul Rhim*,†

Graduate School, Yonsei University
**Department of Mechanical Engineering, Yonsei University*

Abstract : The herringbone groove journal bearing (HGJB) has chevron type grooves on stationary or rotating member of the bearing so that they pump the lubricant inward the grooves when journal rotates. As a result, the pressure is generated around the journal so that the radial stiffness and dynamic stability are improved comparing to the plain journal bearing (PJB) when the bearing operates near the concentric condition. The narrow groove theory, conventionally adopted to simulate the concentric operation of HGJB, is limited to the infinite number of grooves. A numerical study of air-lubricated HGJB is presented for the finite number of grooves. The compressible isothermal Reynolds equation is solved by using Finite Element Method together with the Newton-Raphson iterative procedure and perturbation method. The solutions render the static and dynamic performances of HGJB. Comparison of present results with a PJB validates previously published finite difference solution. The HGJB's geometric parameters influence its static and dynamic characteristics. The optimum geometric parameters are presented for the air-lubricated HGJB in particular conditions.

Key words : Air-lubricated, herringbone groove journal bearing, FEM, perturbation method, static & dynamic characteristics, optimum geometric parameters

Introduction

The herringbone groove journal bearing (HGJB) began to be studied through analysis and experiment from the 1960s [1-3]. HGJB was examined to improve the stiffness and the stability of the bearing for high speed and light loaded operation[4]. Most of analytic studies were conducted based on the "Narrow groove theory", which assumes that there is infinite number of grooves on the bearing system. In 1977, Bootsma and Tielemans accomplished an experimental study of leakage-free operation of HGJB [5]. In these days, researchers attempt to apply HGJB to small size, high precision household electric appliances due to its high rotational stability characteristics [6].

Recently, the HGJB is regarded as an excellent replacement of ball bearings in the spindle system of the computer hard disk drive due to its small non-repeatable run-out (NRRO) and low noise characteristics [7,8]. An NRRO is the one of major sources for the track mis-registration between the read/write head and the disk data track so that it prevents us from achieving high track density in a computer hard disk drive. The fluid film bearing is possible to keep low NRRO because it prevents direct contact between journal and bearing as well as increases radial damping to suppress the vibration. In addition to the above advantages, herringbone grooves pump lubricant toward the center of the chevron, which reduces the side leakage as well as increases the stability of the rotating system in comparison with a plain journal bearing.

A 2-D analysis of HGJBs has been made by Murata, Miyake, Kawabata [9] in which potential flow theory has been applied to the flow of grooved journal bearings. Kobayashi [10] presented a simulation procedure for the orbital motion of the journal by using a multi-grid method with the divergence formulation, as an engineering tool to study both stationary and time-dependent problems of oil-lubricated HGJB.

A number of self-acting bearing designs have evolved that have somewhat stable operating characteristics. These designs shape the bearing surface to create artificial fluid-film wedges in the absence of any applied radial load. The HGJB is one of them. When we calculate the bearing performance there are some geometric parameters for the HGJB as shown in Fig. 1 such as groove angle β, groove width ratio $\alpha = l_g/l$, groove depth ratio $\gamma = h_g/h_r$, number of grooves N, and asymmetric ratio

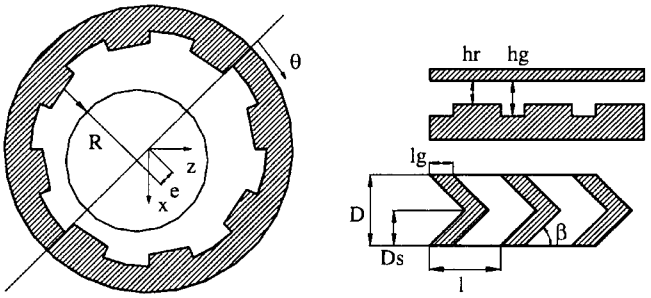

Fig. 1. Configuration of a HGJB and definition of bearing geometric parameters.

†Corresponding author; Tel: 82-2-2123-2820; Fax: 82-2-312-2159
E-mail: rhimyc@yonsei.ac.kr

$\delta = D_g/D$.

In this paper, a numerical study of air lubricated HGJB is presented for the finite number of grooves. A compressible Reynolds equation is solved numerically by using Finite Element Method. The non-linearity of the discretized equations is linearized with the Newton-Raphson procedure. Load capacity, attitude angle, stiffness, damping coefficients, and stability are given for various geometric parameters for the case of smooth member rotating. The goal of this study is finding optimum geometric parameters considering maximum stability of the rotating system.

Air-Lubricated HGJB

Governing Equation

The pressure distribution in a fluid film bearing can be computed by the Reynolds equation which is derived from the Navier-Stokes equations under certain assumptions. Assumptions used in this study are isothermal and isoviscous fluid with perfect gas law, laminar flow with no-slip boundary conditions. The governing equation obtained is the following nonlinear equation:

$$\frac{\partial}{\partial x}\left(ph^3\frac{\partial p}{\partial x}\right)+\frac{\partial}{\partial y}\left(ph^3\frac{\partial p}{\partial y}\right) = 6\mu\left\{U\frac{\partial}{\partial x}(ph)+2\frac{\partial}{\partial t}(ph)\right\}. \quad (1)$$

Before we go further, it is usual to non-dimensionalize the governing equation to examine the bearing characteristics in terms of non-dimensional parameters. When we use dimensional parameters for the governing equation such as ambient pressure p_a, diameter of the bearing $D = 2r$, length of the bearing L, bearing clearance c, viscosity μ, rotational speed $\omega = U/r$, whirl speed ν, then we get dimensionless parameters such as dimensionless coordinates $\theta = x/r$, $\zeta = y/r$, dimensionless pressure $P = p/p_a$, dimensionless film thickness $H = h/c$, bearing number $\Lambda = (6\mu\omega/p_a)(r/c)^2$, dimensionless time $\tau = j\nu t$ $\{j = (-1)^{1/2}\}$, whirl ratio $\gamma_w = \nu/w$, and diameter to length ratio $\lambda = D/L$.

Non-dimensionalized compressible Reynolds equations is obtained by substituting above relations to the Eqn. (1) as following:

$$\frac{\partial}{\partial\theta}\left(PH^3\frac{\partial P}{\partial\theta}\right)+\frac{1}{4}\lambda^2\frac{\partial}{\partial\zeta}\left(PH^3\frac{\partial P}{\partial\zeta}\right) = \Lambda\frac{\partial}{\partial\theta}(PH)+2j\Lambda\gamma_w\frac{\partial}{\partial\tau}(PH). \quad (2)$$

Static and Dynamic Characteristics of a HGJB

In Fig. 2, the film thickness of the herringbone groove journal bearing can be expressed as

$$\begin{pmatrix} H = 1+\varepsilon\cos\theta+H_g \rightarrow Groove\ \ Part \\ H = 1+\varepsilon\cos\theta \qquad\quad \rightarrow Ridge\ \ Part \end{pmatrix}. \quad (3)$$

As the smooth member rotates, we can discard the time term in Eqn. (2) then we can get the steady-state equation as following:

$$\frac{\partial}{\partial\theta}\left(P_oH_o^3\frac{\partial P_o}{\partial\theta}\right)+\frac{1}{4}\lambda^2\frac{\partial}{\partial\zeta}\left(P_oH_o^3\frac{\partial P_o}{\partial\zeta}\right) = \Lambda\frac{\partial}{\partial\theta}(P_oH_o). \quad (4)$$

Integration of the pressure fields from Eqn. (4) over the journal surface gives the fluid film bearing reaction forces and journal attitude angle which are expressed as following:

$$\begin{Bmatrix} F_r \\ F_t \end{Bmatrix} = \frac{1}{p_aLD}\begin{Bmatrix} f_r \\ f_r \end{Bmatrix} = \frac{1}{2}\int_\zeta\int_\theta(P_o-1)\begin{Bmatrix} -\cos\theta \\ \sin\theta \end{Bmatrix}d\theta d\zeta \quad (5)$$

$$\Phi = tan^{-1}\left(\frac{F_t}{F_r}\right)$$

Perturbation method is applied to get dynamic coefficients. The resultant reaction load has components F_x and F_z as shown in Fig. 2. Performing a first-order Taylor expansion of these components gives

$$F_x = (F_x)_0+\Delta F_x$$
$$= (F_x)_0+\left(\frac{\partial F_x}{\partial x}\right)_0\Delta x+\left(\frac{\partial F_x}{\partial z}\right)_0\Delta z+\left(\frac{\partial F_x}{\partial x'}\right)_0\Delta x'+\left(\frac{\partial F_x}{\partial z'}\right)_0\Delta z'$$

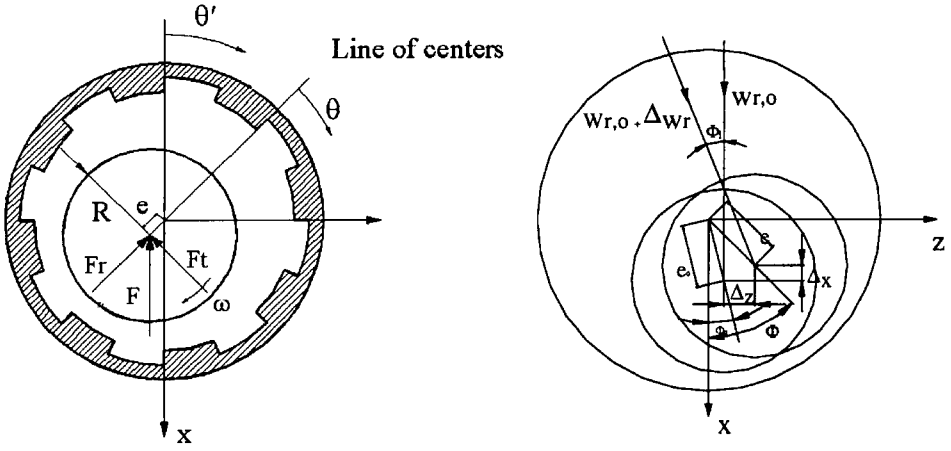

(a) Force components and attitude angle (b) Perturbation of journal center

Fig. 2. Force components and coordinate system of a HGJB.

$$= (F_x)_0 + K_{xx}\Delta x + K_{xz}\Delta z + C_{xx}\Delta x' + C_{xz}\Delta z' \quad (6)$$

$$F_z = (F_z)_0 + \Delta F_z$$

$$= (F_z)_0 + \left(\frac{\partial F_z}{\partial x}\right)_0 \Delta x + \left(\frac{\partial F_z}{\partial z}\right)_0 \Delta z + \left(\frac{\partial F_z}{\partial x'}\right)_0 \Delta x' + \left(\frac{\partial F_z}{\partial z'}\right)_0 \Delta z'$$

$$= (F_z)_0 + K_{zx}\Delta x + K_{zz}\Delta z + C_{zx}\Delta x' + C_{zz}\Delta z' \quad (7)$$

where Δx and Δz are the corresponding whirl amplitudes of the journal in x and z direction, respectively. K $(=\frac{c}{f}k_{ik})$ and C $(=\frac{c\omega}{f}c_{ik})$ are the stiffness and damping coefficients, respectively, when f represents the load capacity and apostrophes represent time derivatives. Recall that the direction of the x axes was chosen so that $(F_z)_0 = 0$, where F represents the dimensionless load defined as $F = \frac{f}{P_a LD} = \sqrt{F_r^2 + F_t^2}$. Equations (6) and (7) can be recast as

$$\begin{pmatrix} F_x \\ F_z \end{pmatrix} = \begin{pmatrix} (F_x)_0 \\ 0 \end{pmatrix} + \begin{bmatrix} K_{xx} & K_{xz} \\ K_{zx} & K_{zz} \end{bmatrix} \begin{pmatrix} \Delta x \\ \Delta z \end{pmatrix} + \begin{bmatrix} C_{xx} & C_{xz} \\ C_{zx} & C_{zz} \end{bmatrix} \begin{pmatrix} \Delta x' \\ \Delta z' \end{pmatrix} \quad (8)$$

If smooth member rotates, perturbed film thickness can be expressed as follows using Eqn. (3) and $\theta' = \theta + \Phi$.

$$H = H_0 + \left(\frac{\partial H}{\partial x}\right)_0 \Delta x + \left(\frac{\partial H}{\partial z}\right)_0 \Delta z = H_0 + \cos\theta\,'\Delta x + \sin\theta\,'\Delta z \quad (9)$$

Equation (8) is valid when the journal motion is harmonic. The whirl amplitude of journal and its derivative can be written in complex form as $\Delta x = \mathrm{Re}\{\varepsilon_1 \exp^{j\nu t}\}$ and $\Delta x' = \mathrm{j}\ Dx = \mathrm{Re}\{\mathrm{j}\varepsilon_1 \exp^{j\nu t}\}$, respectively. Consider a similar first-order expansion of the pressure,

$$P = P_0 + \left(\frac{\partial P}{\partial x}\right)_0 \Delta x + \left(\frac{\partial P}{\partial z}\right)_0 \Delta z + \left(\frac{\partial P}{\partial x'}\right)_0 \Delta x' + \left(\frac{\partial P}{\partial z'}\right)_0 \Delta z' . \quad (10)$$

Let the journal center have a static eccentricity ratio ε_0 with a corresponding attitude angle Φ_0. This position is perturbed by a small amount of motion due to the translation motion of the journal: $(\varepsilon_1, \varepsilon_0\ \Phi_1)$. The corresponding perturbed forms of the dimensionless pressure and film thickness can be written as:

$$P = P_0 + \varepsilon_1 e^{j\nu t} P_1 + \varepsilon_0 \Phi_1 e^{j\nu t} P_2 , \quad (11)$$

$$H = H_0 + \varepsilon_1 e^{j\nu t} \cos\theta + \varepsilon_0 \Phi_1 e^{j\nu t} \sin\theta . \quad (12)$$

These two equations are substituted into Eqn. (2) to get equations related to P_1 and P_2, which are linear equations with complex dependent variables. They can be solved numerically once steady-state solution P_0 is obtained. The dynamic coefficients, stiffness and damping coefficients, can be expressed as follows:

$$\begin{bmatrix} K_{xx} & K_{xz} \\ K_{zx} & K_{zz} \end{bmatrix} = \frac{c}{P_a LD} \begin{bmatrix} k_{xx} & k_{xz} \\ k_{zx} & k_{zz} \end{bmatrix} = -\frac{1}{2}\int_\zeta \int_\theta Re\left\{ \begin{bmatrix} P_1 \cos\theta\,' & P_2 \cos\theta\,' \\ P_1 \sin\theta\,' & P_2 \sin\theta\,' \end{bmatrix} \right\} d\theta d\zeta \quad (13)$$

$$\begin{bmatrix} C_{xx} & C_{xz} \\ C_{zx} & C_{zz} \end{bmatrix} = \frac{c\omega}{P_a LD} \begin{bmatrix} c_{xx} & c_{xz} \\ c_{zx} & c_{zz} \end{bmatrix} = -\frac{1}{2}\int_\zeta \int_\theta Im\left\{ \begin{bmatrix} P_1 \cos\theta\,' & P_2 \cos\theta\,' \\ P_1 \sin\theta\,' & P_2 \sin\theta\,' \end{bmatrix} \right\} d\theta d\zeta \quad (14)$$

The boundary conditions for the governing and perturbed equations are ambient pressure at both ends in axial direction and periodic in circumferential direction, i.e.,

$$P_0 = 1,\ P_1 = 0,\ P_2 = 0 \quad \text{at} \quad Y = 0,\ 1, \quad (15)$$

$$P_0(\theta, \zeta) = P_0(\theta + 2\pi, \zeta), \quad P_1(\theta, \zeta) = P_1(\theta + 2\pi, \zeta),$$
$$P_2(\theta, \zeta) = P_2(\theta + 2\pi, \zeta) \quad (16)$$

Stability Conditions

Two kinds of dynamic instabilities may be found in fluid film bearings. Since the gas film has lower damping properties than the liquid film, these instabilities in gas-lubricated bearings become more prominent than with liquid-lubricated bearings. The one is associated with typical spring-mass natural frequencies where the bearing fluid-film is the spring. The other is a self-excited vibration characterized by having the center of the shaft orbit around the center of the bearing at some frequency equal to or somewhat less than one half of the spinning or rotational velocity of the shaft. Under these conditions, the capacity of the bearing to support radial load is sharply reduced and may fall to zero. The shaft system may be stable as the speed is increased until this threshold is reached. Crossing this threshold through further, unlike an ordinary critical speed, the shaft cannot pass through this one and attain a region of stability on the other side at a higher speed.

States of neutral stability exist (for the case of the journal bearing) at those whirl speeds where the tangential component of the fluid film force vanishes, and when the centrifugal force, due to whirl, is in equilibrium with the radial component of the fluid force. At this point of neutral stability a critical mass of the rotor may be determined. If the rate of change the radial force component of the fluid film with respect to the rotor spin speed becomes negative, the system will go unstable, and of course if the derivative is positive the system will remain stable.

If the system load is stationary, $F = (F_x)_0$, then the equations of motion for the constant speed journal mass m_a can be derived in x and z direction, respectively by applying small perturbations Δx and Δz on the equilibrium position. A set of non-dimensionalized equation of motion is obtained as following:

$$-\gamma_w^2\begin{bmatrix}M_a & 0\\ 0 & M_a\end{bmatrix}\begin{pmatrix}\Delta x''\\ \Delta z''\end{pmatrix}+j\gamma_w\begin{bmatrix}C_{xx} & C_{xz}\\ C_{zx} & C_{zz}\end{bmatrix}\begin{pmatrix}\Delta x'\\ \Delta z'\end{pmatrix}+\begin{bmatrix}K_{xx} & K_{xz}\\ K_{zx} & K_{zz}\end{bmatrix}\begin{pmatrix}\Delta x\\ \Delta z\end{pmatrix}=\begin{pmatrix}0\\ 0\end{pmatrix} \tag{17}$$

where, $\mathrm{Ma}=\dfrac{cm_a\omega^2}{f}$ and γ_w is the whirl ratio defined as $\gamma_w=\dfrac{v}{\omega}$. For a given eccentricity ratio, homogeneous solutions to Eqn. (17) corresponding to the unstable root may be $\Delta x = x_h\exp(\tau)$ and $\Delta z = z_h\exp(\tau)$. Substituting these solutions into equation (17) gives:

$$\begin{bmatrix}-\gamma_w^2+M_a+K_{xx}+j\gamma_x C_{xx} & K_{xz}+j\gamma_x C_{xz}\\ K_{zx}+j\gamma_x C_{zx} & -\gamma_w^2+M_a+K_{zz}+j\gamma_x C_{zz}\end{bmatrix}\begin{pmatrix}x_h\\ z_h\end{pmatrix}exp^{\tau}=\begin{pmatrix}0\\ 0\end{pmatrix}. \tag{18}$$

Thus either $x_h = z_h = 0$, which is the trivial steady-state solution, or determinant of above equation must be zero, which is for the nontrivial solution. This gives the information for the stability criteria for the rotor system as follows:

$$(K_{xx}-\gamma_w^2(M_a)_{cr})(K_{zz}-\gamma_w^2(M_a)_{cr})-\gamma_w C_{xx}\gamma_w C_{zz}-K_{xz}K_{zx}+\gamma_w C_{xz}\gamma_w C_{zx}=0 \tag{19}$$

$$(M_a)_{cr}=\frac{K_{xx}\gamma_w C_{zz}+K_{zz}\gamma_w C_{xx}-K_{xz}\gamma_w C_{zx}-K_{zx}\gamma_w C_{xz}}{\gamma_w^2(\gamma_w C_{xx}+\gamma_w C_{zz})} \tag{20}$$

where, $(M_a)_{cr}$ is the dimensionless critical mass parameter normalized as $(M_a)_{cr}=\left(\dfrac{cm_a\omega^2}{f}\right)_{cr}$.

Using an initial guess of 0.5 for the whirl ratio γ_w, the dimensionless critical mass $(M_a)_{cr}$ is found from the Eqn. (20) and is substituted into the Eqn. (19). In general, there will be a residue. Then an adjustment in the whirl ratio is made to minimize the residue. The procedure is repeated until the residue has become sufficiently small.

If M_a is smaller than $(M_a)_{cr}$, the system will be stable, but it will be unstable for M_a larger than $(M_a)_{cr}$. Thus, whether the bearing is susceptible to instability obviously depends on the values of the bearing coefficients, which in turn depend on the bearing type and the various performance parameters to describe the film thickness.

Numerical Analysis

In this study, we have used the Bubnov-Galerkin's method which employs the same function for the weighting function that is used in the approximating equation. To obtain the static pressure distribution of air-lubricated journal bearing, we can use Eqn. (4). First, we define residual equation for Eqn. (4) multiplied by a suitable weighting function [N] as follows:

$$W(P_0)=\int_\Lambda [N]^T\left\{\frac{\partial}{\partial\theta}\left(P_0H_0^3\frac{\partial P_0}{\partial\theta}\right)+\frac{1}{4}\lambda^2\frac{\partial}{\partial\zeta}\left(P_0H_0^3\frac{\partial P_0}{\partial\zeta}\right)-\Lambda\frac{\partial}{\partial\theta}(P_0H_0)\right\}dA=0. \tag{21}$$

Integrating by parts over a subdomain, employing the Green-Gauss Theorem, and applying boundary conditions given in Eqn. (15) and (16) becomes

$$W(P_0)=\int_\Lambda\left\{P_0H_0^3\left[\left(\frac{\partial N}{\partial\theta}\frac{\partial P_0}{\partial\theta}+\frac{1}{4}\lambda^2\frac{\partial N}{\partial\zeta}\frac{\partial P_0}{\partial\zeta}\right)\right]-P_0H_0\Lambda_X\frac{\partial N}{\partial\theta}\right\}dA=0. \tag{22}$$

Newton-Raphson iteration procedure can be employed to solve Eqn. (22), a nonlinear integro-differential equation. Beginning with an initial guess of $P_0^{(0)}$, Newton-Raphson method may be used to construct a sequence of $P_0^{(1)}$, $P_0^{(2)}$, etc. as $P_0^{(n+1)}=P_0^{(n)}+\Psi^{(n)}$ where, $\Psi^{(n)}$ is a solution of the linear problem of $W'(P_0^{(n)})\Psi^{(n)}+W(P_0^{(n)})=0$. Here, $W'(P_0^{(n)})$ is the Frechet derivative of $W(P_0^{(n)})$ with respect to P_0 evaluated at $P_0=P_0^{(n)}$. If it exists, this linear operator is defined by:

$$W'(P_0^{(n)})\psi^{(n)}=\lim_{\varepsilon\to 0}\left(\frac{d}{d\varepsilon}W(P_0^{(n)}+\varepsilon\psi^{(n)})\right). \tag{23}$$

The final discretized equation for each element can then be obtained as:

$$[K_1^{(n)}-K_2]\{\psi^{(n)}\}=\{F^{(n)}\} \tag{24}$$

where

$$[K_1^{(n)}]=\left[\int_A\left\{\left(P_0^{(n)}H_0^3\left(\frac{\partial N^T}{\partial\theta}\frac{\partial N}{\partial\theta}+\frac{1}{4}\lambda^2\frac{\partial N^T}{\partial\zeta}\frac{\partial N}{\partial\zeta}\right)+[N]H_0^3\left(\frac{\partial N^T}{\partial\theta}\frac{\partial P_0^{(n)}}{\partial\theta}+\frac{1}{4}\lambda^2\frac{\partial N^T}{\partial\zeta}\frac{\partial N_0^{(n)}}{\partial\zeta}\right)\right)\right\}dA\right],$$

$$[K_2] = \left[\int_A \left(H_0 \Lambda_X \frac{\partial N^T}{\partial \theta}[N]\right) dA\right], \tag{40}$$

$$\{F^{(n)}\} = \left\{-\int_A \left[P_0^{(n)} H_0^3 \left(\frac{\partial N}{\partial \theta}\frac{\partial P_0^{(n)}}{\partial \theta} + \frac{1}{4}\lambda^2 \frac{\partial N}{\partial \zeta}\frac{\partial P_0^{(n)}}{\partial \zeta}\right) - P_0^{(n)} H_0 \Lambda_X \frac{\partial N}{\partial \theta}\right] dA\right\}.$$

Eight node quadrilateral elements are used for the computation. Three points Gaussian quadrature is employed for the numerical integration and under-relaxation is used for the stable iteration. Integration of the dynamic pressure field (P_1 and P_2) on the bearing surface gives stiffness (real part) and damping (imaginary part) coefficients.

Results and Discussion

In order to verify the developed FEM code, some steady-state results for a plain cylindrical gas-lubricated journal bearing (Raimondi [11]) are compared with results from present analysis. The code is able to accommodate a plain cylindrical bearing by simply equating the groove depth γ to 1.0. Here the bearing length to diameter ratio L/D is set to 1.0.

Figure 3 presents the dimensionless load capacity F and the attitude angle Φ, as a function of bearing number Λ for an L/D ratio of one and eccentricity ratio ε is 0.4. The present FEM solutions coincide very well with Raimondi's solutions.

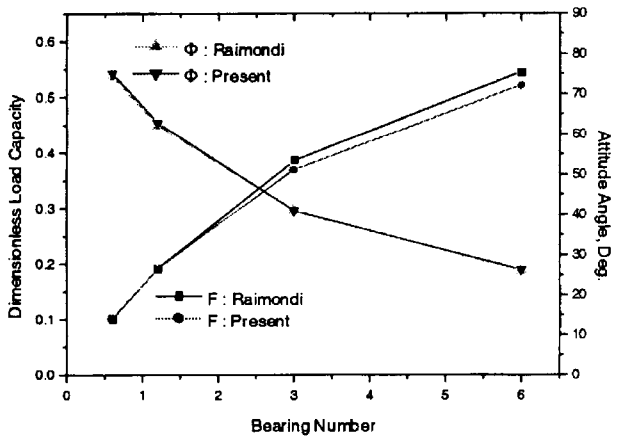

Fig. 3. Comparison of load and attitude angle for various bearing number (ε=0.4).

Figure 4 presents the pressure distribution of a PJB and a HGJB for the bearing number $\Lambda = 5.0$ and eccentricity ratio $\varepsilon = 0.3$, respectively. The geometric parameters of a HGJB are groove angle $\beta = 30°$, groove width ratio $\alpha = 0.5$, groove depth ratio $\gamma = 2.0$, and number of grooves $N = 8$. In Fig. 4(a), there are negative pressure regions but in Fig. 4(b), due to the grooves, there is a pressure generated in negative pressure regions of a PJB.

Figure 5 and 6 show a comparison of the dimensionless stiffness coefficients and damping coefficients with a PJB and a HGJB as a function of eccentricity ratio, respectively. The dynamic coefficients are non-dimensionalized by a load carrying capacity F at each eccentricity ratio. The direct stiffness values K_{xx} and K_{zz} become larger as the eccentricity decrease. These characteristics of the HGJB are due to the existence of a pressure rise even with zero eccentricity, as shown in Fig. 4.

Also, in Fig. 7 show the attitude angle of journal, load capacity, stiffness, and damping of air-films using incompressible algorithm. The incompressible algorithm is not expected to give accurate characteristics of air-films. The figure shows that large discrepancies occur between incompressible algorithm and compressible algorithm. Thus, the incompressible algorithm cant predict the air-film characteristics correctly.

The characteristics of HGJB vary greatly by geometric parameters. As shown in Fig. 1, these parameters are groove angle β, groove width ratio α, groove depth ratio γ, bearing length to diameter ratio L/D, and groove asymmetric ratio δ. There should be a set of optimum design parameters of HGJB from the view point of stability criteria. However, the general optimal values for the geometric parameters are not proposed

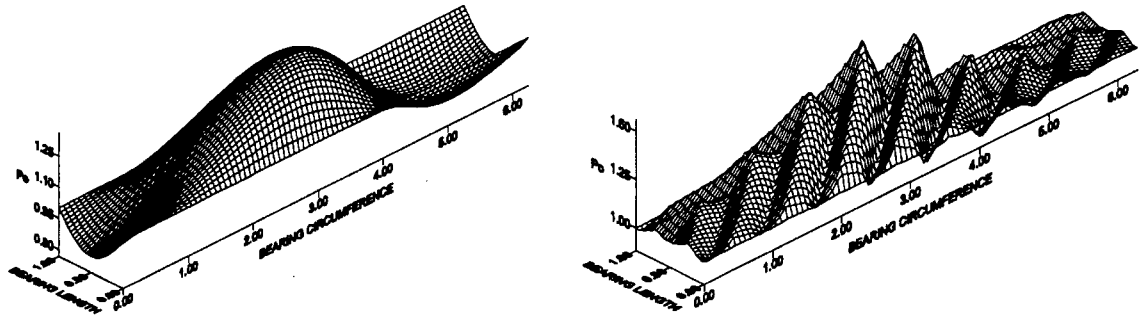

(a) PJB (Λ=5, ε=0.3, L/D=1.0) (b) HGJB (Λ=5, ε=0.3, L/D=1.0)

Fig. 4. The pressure distribution on a bearing surface for 8 grooves.

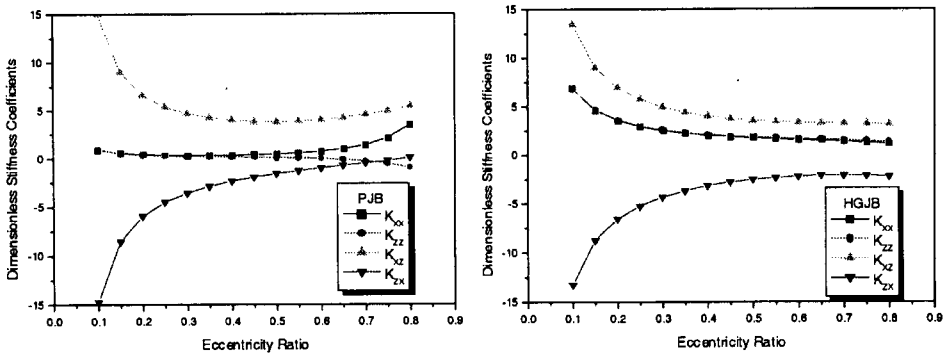

(a) Plain Journal Bearing (b) Herringbone groove Journal Bearing

Fig. 5. Dimensionless stiffness coefficients variations for eccentricity ratios.

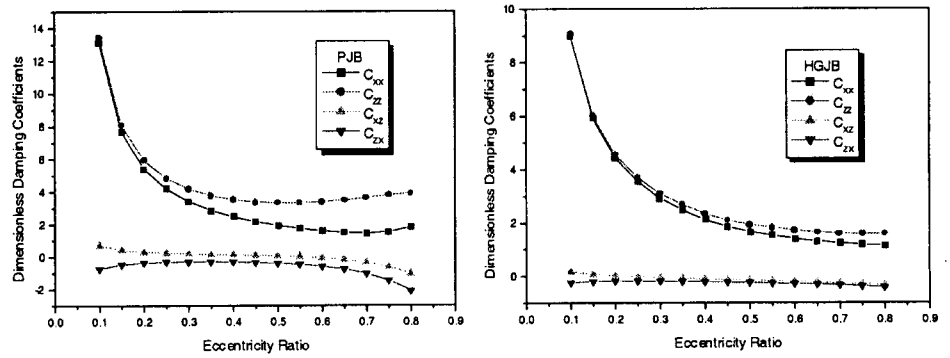

(a) Plain Journal Bearing (b) Herringbone groove Journal Bearing

Fig. 6. Dimensionless damping coefficients variations for eccentricity ratios.

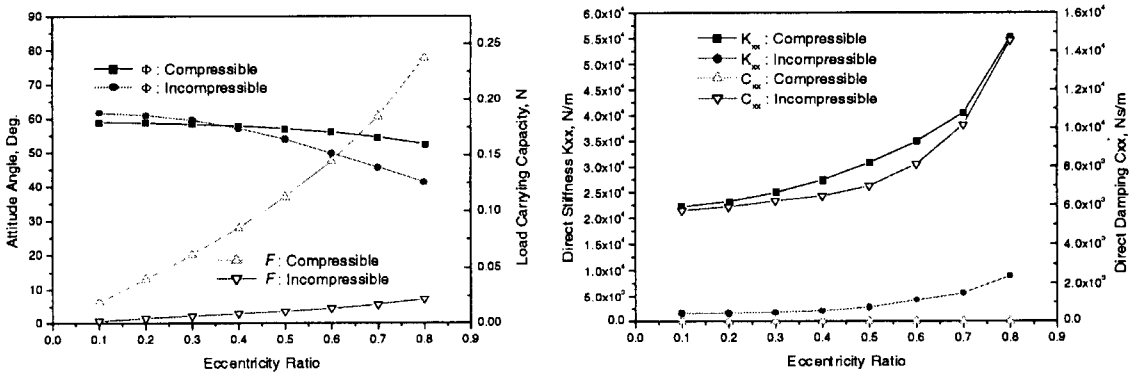

(a) attitude angle and load variations (b) stiffness and damping coefficients variations

Fig. 7. Comparison of compressible and incompressible algorithm.

in this study, which consider cross-related effects between those parameters. The effect of single geometric parameter to the stability is examined instead.

We assume that the objective bearing system is in a steady state and consists of smooth rotor and a fixed sleeve on which eight grooves are formed, where groove angle $\beta = 30$deg., groove width ratio $\alpha = 0.5$, groove depth ratio $\gamma = 2.0$, bearing length to diameter ratio L/D = 1, and groove asymmetric ratio $\delta = 0.5$ with two value of bearing number $\Lambda = 0.2$ and $\Lambda = 2.0$. Examinations are conducted mainly for the eccentricity ratio which is the key variable of most journal bearing analysis.

The dimensionless critical mass variations for eccentricity ratio are given in Fig. 8. The critical mass has a maximum value for the groove angle of 20 deg. when the bearing number is 0.2. However, the maximum value seems to be occurred at less groove angle of 20 deg. as the bearing number increases even in small eccentricity as shown in Fig. 8(b). Generally speaking for highly compressible lubricant as air, the stability decreases gradually as the groove angle increases.

As shown in Fig. 1, the groove width ratio is defined as $\alpha = l_g/l$. Thus, when the groove ratio $\alpha = 0.5$, the land and groove widths are equal. As the groove width ratio decreases,

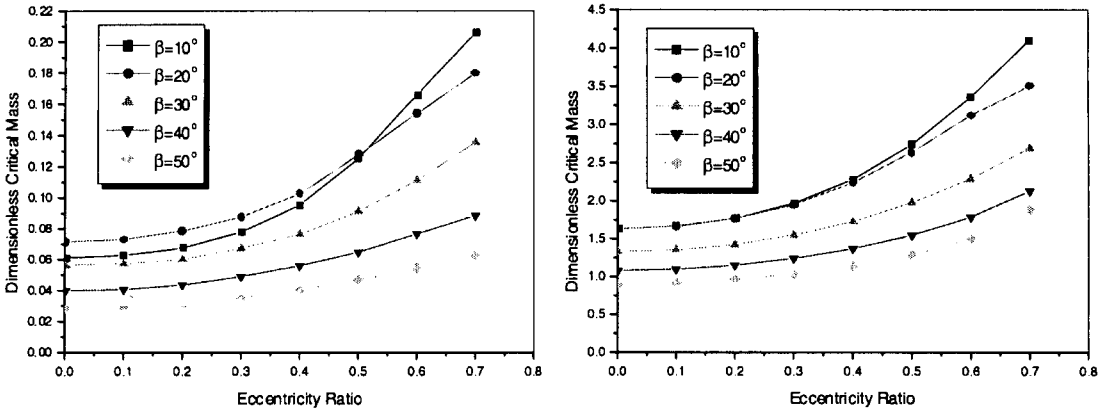

(a) Bearing number Λ=0.2 (b) Bearing number Λ=2.0

Fig. 8. Dimensionless critical mass for various eccentricity ratio.

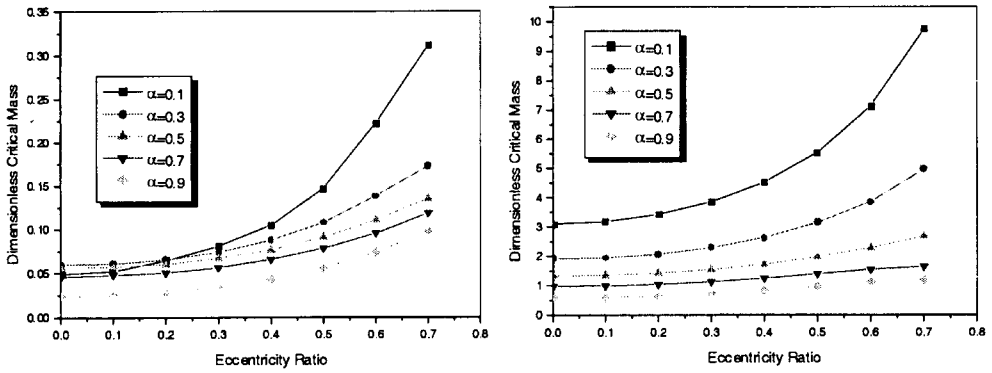

(a) Bearing number Λ=0.2 (b) Bearing number Λ=2.0

Fig. 9. Dimensionless critical mass for various groove width ratio.

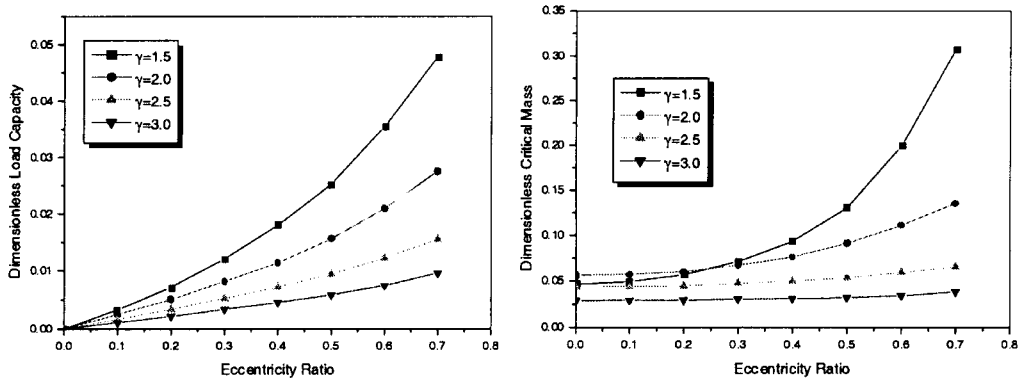

(a) Dimensionless load capacity variation (b) Dimnesionless critical mass variation

Fig. 10. Effect of groove depth for the eccentricity for the bearing number Λ=0.2.

the groove becomes wide so that the load carrying capacity decreases. The dimensionless critical mass variations for the eccentricity ratio are given Fig. 9 for various groove width ratio and two different bearing number, $\Lambda = 0.2$ and $\Lambda = 2.0$. As the bearing number increases, the maximum dimensionless critical mass is obtained for small groove width ratio throughout the eccentricity ratio. However, the load carrying capacity itself becomes smaller as the groove width ratio decreases since the mean effective radial clearance becomes larger for small groove width ratio. Therefore, it is not always the best solution to pursue the maximum dimensionless critical mass for the rotor system.

As shown in Fig. 1, the groove depth ratio $\gamma = 1$ means a plain journal bearing. Figure 10 shows the variations of the dimensionless load capacity and the critical mass for the eccentricity ratio using the groove depth ratio as a parameter. The dimensionless critical mass has its maximum value when the groove depth is the same as the bearing clearance, i.e.,

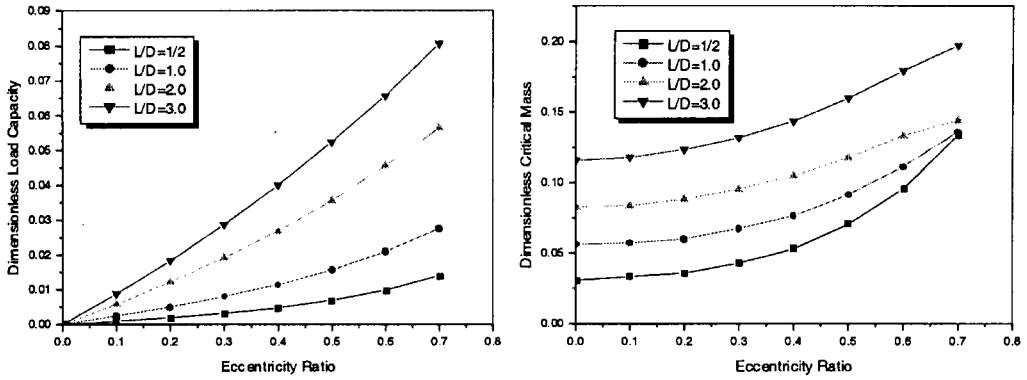

(a) Dimensionless load capacity variation (b) Dimnesionless critical mass variation

Fig. 11. Effect of length to diameter ratio for the eccentricity for the bearing number Λ=0.

γ= 2.0 for the bearing number $\Lambda = 0.2$. However, as the bearing number increases, the groove depth ratio approaches to unity for the maximum critical mass as well as for the maximum dimensionless load capacity.

As the groove depth ratio increases, the mean effective radial clearance increases so that load capacity decreases same as the groove width ratio decreases.

Figure 11 shows the effect of the L/D ratio on dimensionless load capacity and critical mass with respect to the eccentricity ratio. As the L/D ratio increases, the dimensionless load capacity increases faster with eccentricity ratio but the critical mass increase slowly for small eccentricity range and then increases faster for high eccentricity region. Since the critical mass is normalized with the bearing load capacity we have to pay special attention to the variation of the dimensionless critical mass. It has quite high value for high L/D ratio but it doesn't mean that longer bearing is more stable than shorter bearing because longer bearing has high load capacity.

Considering the effect of geometric parameters on the bearing performance, it is not possible to propose an optimal set of geometric parameters for the HGJB. Some applications using HGJB have vertical shafts with light loads, and hence, bearing instability is the major concern especially for the operation with small eccentricity ratio. With the discussions mentioned above, HGJB has superior characteristics to plain journal bearing. However, all the geometric parameters related to the HGJB can be determined case by case depend on the geometrical constraints of the bearing system as well as the operation condition at which the bearing is supposed to run. The software developed in this study can provide appropriate set of geometric parameters for the given conditions and can make the criterion for stable operation.

Conclusions

In the present research, the static and dynamic characteristics for the effects of geometric parameters of HGJB have been investigated using FEM and perturbation methods. We analyze the isothermal compressible fluid flow in herringbone groove journal bearing using Reynolds equation for laminar, inertialess flow. The compressible Reynolds equation is solved by the Bubnov-Galerkin weighted residual method. The non-linear discretized equations is computed with the Newton-Raphson iteration procedure. A simulation tool based on the Finite Element Method is developed to predict the static and dynamic performances of the HGJB. Comparisons of the present steady-state solutions given for a plain cylindrical bearing with published numerical results confirmed the validity of the FEM code. The following conclusions are drawn.

1. The development of significant direct stiffness while running concentrically proves the distinct advantage of using the HGJB over plain journal bearings. Thus the herringbone groove journal bearing is more stable than the plain journal bearing at nearly concentric operation.
2. Using a geometry with 8 grooves for bearing number $\Lambda = 0.2$ during nearly concentric operation, the optimum geometric parameters of HGJB are groove angle $\beta = 20$ deg, groove width ratio $\alpha = 0.3$, groove depth ratio $\gamma = 2.0$, and L/D ratio of 1.5. These values yield a maximum stability at nearly concentric position.
3. As the groove angle β increases, the stability and load capacity decrease. Since the grooves become shorter supplying less bearing area for the pressure to develop.
4. The load capacity generally decreases as the grooves become wide or deep, since in all of these cases the mean effective radial clearance becomes large.

Acknowledgment

This work was funded by the Korea Science and Engineering Foundation (KOSEF) through the Center for Information Storage Device(CISD) Grant No. 2000G0201.

References

1. Vohr, J. H. and Chow, C. Y., 1965, Characteristics of Herringbone-Grooved Gas Lubrication Journal Bearings, ASME Journal of Basic Engineering, Vol. 87, pp. 568-578.
2. Malanoski, S. B., 1967, Experiments on an Ultrastable Gas Journal Bearing, ASME Journal of Lubrication Technology, Vol. 89, No. 4, pp. 433-438.
3. Cunningham, R. E., Fleming, D. P. and Anderson, W. J., 1969, Experimental Stability Studies of the Herringbone

Grooved Gas-Lubricated Journal Bearings, ASME Journal of Lubrication Technology, pp. 52-59.
4. Cunningham, R. E., Fleming, D. P. and Anderson, W. J., 1971, Experimental Load Capacity and Power Loss of Herringbone Grooved Gas Lubricated Journal Bearings, ASME Journal of Lubrication Technology, pp. 415-422.
5. Bootsma, J. and Tielemans, L. P. M., 1977, Conditions of Leakage-Free Operation of Herringbone Grooved Journal Bearings, ASME Journal of Lubrication Technology, Vol. 99, pp. 215-223.
6. Tanaka, K. and Muraki, H., 1991, Performance of Air-Lubricated Hydrodynamic Bearing Spindles for Laser Scanners, ASME Journal of Tribology, Vol. 113, pp. 609-614.
7. Kenneth A. Liebler, 1995, Future Trends in Spindle Bearing for Disk Drives, DATA STORAGE, November/December, pp. 37-40.
8. Ono, K., Zhu, J. and Cui, C., 1997, A Comparison Study on the Characteristics of Five Types of Hydrodynamic Oil Bearings for Hard Disk Spindles, International Conference on Micromechatronics for Information and Precision Equipment, Tokyo, Japan, MR-02, pp. 20-25.
9. Murata, S., Miyake, Y. and Kawabata, N., 1980, Two-Dimensional Analysis of Herringbone Grooved Journal Bearings, Bulletin of JSME, Vol. 23, pp. 1220-1227.
10. Kobayashi, T., 1999, Numerical Analysis of Herringbone-Grooved Gas-Lubricated Journal Bearings Using a Multigrid Technique, ASME Journal of Tribology, Vol. 121, pp. 148-155.
11. Raimondi, A. A., 1961, A Numerical Solution for Gas-Lubricated Full Journal Bearing of Finite Length, Transaction ASLE, Vol. 4, pp. 131-155.